Polymer 51 (2010) 1608–1613

Contents lists available at ScienceDirect

Polymer

journal homepage: www.elsevier.com/locate/polymer

Effect of network structure on the stress–strain behaviour of endlinked PDMS elastomers

Seong Hyun Yoo, Leslie Yee, Claude Cohen*

School of Chemical and Biomolecular Engineering, Olin Hall, Cornell University, Ithaca, NY 14853, USA

ARTICLE INFO

Article history:
Received 10 August 2009
Received in revised form
27 January 2010
Accepted 31 January 2010
Available online 8 February 2010

Keywords:
Elastomers
Stress–strain behaviour
Entanglement

ABSTRACT

Endlinked poly(dimethylsiloxane) (PDMS) networks synthesized from telechelic precursor chains of different molar mass were prepared with varying volume fractions of non-reactive chains acting as solvent. Uniaxial extension and compression measurements were performed on these networks to investigate their stress–strain behaviour. The effect of the network structure and of solvent on the stress–strain behaviour is examined by controlling the extent of crosslinks and entanglements during the network synthesis. The master curve of the Rubinstein and Panyukov non-affine slip-tube (NAST) model provide an adequate fit to most of the extension and compression data. Furthermore, the crosslink and entanglement parameters of the NAST model (G_c and G_e) are found to be in general in reasonable agreement with the $2C_1$ and $2C_2$ parameters of the Mooney–Rivlin continuum model applied to the extension data. For high molar mass precursor chains, the entanglement contribution to the modulus surpasses the crosslink contribution.

1. Introduction

Ideal rubber elasticity in uniaxial extension is represented by the expression:

$$\sigma = G\left(\alpha - \alpha^{-2}\right) \tag{1}$$

where σ is the engineering stress (force/original cross-section area), G is the elastic shear modulus of the material, and α is the extension ratio. In the absence of crystallization, the curve of experimental engineering stress data versus the extension ratio can be thought of as consisting of three regions: low extension ratios where the experimental data follow Eq. (1), moderate extension ratios where the experimental stress data fall below the prediction of Eq. (1), and high extension ratios where Eq. (1) may start to underpredict the experimental stress values. It has been common to associate the initial deviation at moderate extension ratios to chain interactions (e.g., the slippage of entanglements between elastic chains) and deviations at high extensions to the breakdown of the Gaussian coil assumption and the finite extensibility of a polymer chain [1]. It has been shown that the inverse Langevin equation gives a good description of the end-to-end length of a single stretched chain and it has been used to correct for the large stress increase at high extension [1]. We concern ourselves here with the moderate extension regime dominated by chain–chain interactions that cause the experimental values of the stress to lie below the ideal rubber elasticity prediction once the modulus is fitted experimentally. We use endlinking chemistry to synthesize controlled polymeric network structures which provide a unique opportunity to test various models of rubber elasticity that predict the elastic modulus, equilibrium swelling, and chain segment orientation of deformed networks [2]. The elastic modulus represents only the behaviour at small deformation in uniaxial extension measurements. The role of the network structure governed by the degree of crosslinking, entanglement, and solvent concentration on the elastic modulus (low strain data) has been extensively studied in the past [3]. Here, we examine the less known role of the network structure on the stress–strain behaviour at moderate elongation where deviation from ideal rubber elasticity occurs. We show that using the fitted parameters of the coarse-grained non-affine slip-tube model [4] allows for a physical interpretation of the different molecular effects that lead to deviation from the ideal rubber elasticity and permits an evaluation of the effects of the preparation conditions on the ensuing structure of the network. To accomplish this, we examined the effects of the precursor molar mass, the reactive polymer content during curing, and the presence of a solvent on the stress–strain curves.

* Corresponding author.
E-mail address: cc112@cornell.edu (C. Cohen).

0032-3861/$ – see front matter © 2010 Elsevier Ltd. All rights reserved.
doi:10.1016/j.polymer.2010.01.067

2. Experimental procedure

Telechelic vinyl-terminated polydimethylsiloxane chains and endlinked networks were synthesized by standard methods previously published [5–10]. In brief, the PDMS polymer chains were synthesized by anionic polymerization of hexamethylcyclotrisiloxane (D_3) in toluene, using dimethyl sulfoxide as a promoter and benzyltrimethylammonium bis(o-phenylenedioxy)phenylsiliconate as a catalyst. Calculated amounts of water were added to control the molar mass of the resulting polymer. After the polymerization, pyridine (an acid scavenger) was added to the resulting polymer/toluene mixture. The living chains were end-capped with vinyl groups by adding vinyldimethylchlorosilane. The polymer samples thus obtained were washed with water, dissolved and re-precipitated with toluene and methanol, and then dried in a vacuum oven at 60 °C for 3 days.

The precursor molar masses were characterized by gel permeation chromatography and determined to be 10,000, 30,000 and 80,000 g/mol (rounded-off to the nearest 1000). A well established conversion was used to obtain the PDMS molar masses from polystyrene equivalents [11]. The polydispersities of the samples were below 1.3. The networks were prepared in a series of different initial precursor polymer concentrations ($\phi = 0.3$ to 1) to vary the extent of trapped entanglements. The solvent used was an unreactive trimethoxy-terminated PDMS of molar mass 6000/mol. For the molar masses of the reactive chains considered here, this solvent acts as a theta solvent [12].

After the networks were cured, they were removed from the moulds and a sample puncher was employed to produce test pieces of uniform width and thickness. Typical samples were 0.5–1 mm thick and 4.3 mm wide. We measured engineering stress (force/initial cross-sectional area) versus extension ratio (length/initial length) with an Instron machine (model 1125) with the uniaxial extension setup. The distance between the two clamps was 40–45 mm. The samples were clamped in their unstrained state at room temperature and extended at 20 mm/min until fracture. This strain rate was selected after verifying that the stress–strain data were independent of strain rate at this slow extension speed. Young's modulus (E) was determined by calculating the slope of the best fit line through the first 5% of the stress–strain curve, where the trend is linear. For PDMS networks, the value of E was previously found to be three times that of G [13]. Compression data were obtained in similar fashion using the Instron uniaxial compression setup. All samples were tested both in the prepared (swollen state) and in the dry state obtained by extracting the solvent with toluene and drying the samples. Thus, the effects of a wide range of trapped entanglements and interspersion upon deswelling can be evaluated. The soluble fractions were calculated from the weights of the prepared and dried networks after taking into account the amount of solvent initially present.

3. Results and discussion

3.1. Stress–strain curves in uniaxial extension

To consider the effect of interspersion of chains after solvent removal on the stress–strain behaviour, we compare networks of the three precursor chains endlinked in the presence of a large amount of the unreactive solvent. Fig. 1a shows the stress normalized by the Young's modulus for the networks prepared at $\phi = 0.4$ versus the extension ratio plotted in double-logarithmic plots and Fig. 1b the corresponding results for the dried networks. Note that the overlap concentration ϕ^* of the 10 k chains can be estimated to be roughly 0.2 [12] which indicates that these chains in the preparation state are very marginally interspersed. On the other hand, the 80 k chains have $\phi^* \approx 0.07$ and are highly interspersed in the preparation state. These endlinked networks contain a large amount of trapped entanglements. The effect of these trapped entanglement on the deviation of the stress–stain behaviour from ideal rubber elasticity is evident in Fig. 1a, where the 0.4 swollen 10 k network behaves almost ideally whereas the 30 k and 80 k networks deviates increasingly as a function of the precursor molar mass. The results of Fig. 1b are also quite revealing in that upon drying the 80 k network, a much larger extent of

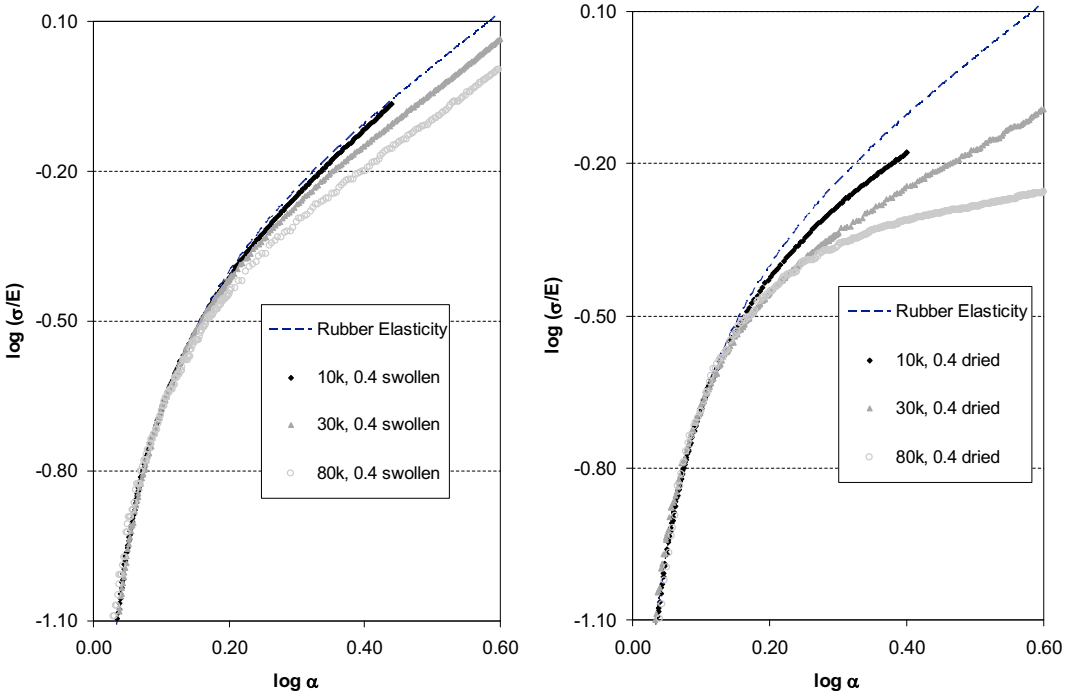

Fig. 1. Log–log plots of normalized stress versus extension ratio for networks of different precursor molar mass: a) Left, networks as prepared at $\phi = 0.4$; b) right, dried networks.

deviation from ideality occurs. Going from the swollen state to the dry state, two factors can affect the increased deviation from ideality: i) the solvent removal increases the effect of the trapped entanglement between interpenetrated elastic chains, and ii) chain interpenetration occurs to achieve dry density and leads to an increase in chain interactions. A much larger extent of interpenetration is expected in the 80 k network as compared to the 10 k network. In other words, the volume encompassed by an elastic chain at melt density in the 80 k network contains many more chains than the volume encompassed by an elastic chain in the 10 k network. This interpenetration of chains upon drying a network leads to non-trapped entanglements between chains that can have a large effect on deviation from the ideal rubber elastic behaviour.

A comparison between the results of swollen and dried networks of same molar mass precursors prepared under different solvent concentration provide clues regarding the effect of solvent and the effect of chain interspersion on deviation from ideal elastic behaviour. Fig. 2 exhibits some of the data for the 30 k networks. The results for $\phi = 0.4$ in Fig. 1 are not duplicated here for clarity, but the data from the 0.4 swollen network fall between the 0.3 and 0.7 swollen data, whereas the data from the 0.4 dried network fall on top of the other two sets of dried data. We see that the 0.3 swollen data deviates only slightly from the ideal rubber behaviour.

As in the case of the 10 k, 0.4 swollen data, we can interpret this result as indicating that the chains do not strongly interact as the network is stretched (ideality assumption). A quantitative analysis of both extension and compression data based on the non-affine slip-tube (NAST) model is presented in Section 3.2 below. It indicates that an appreciable contribution to the modulus of the 0.3 swollen network (~25%) still come from entanglements. As this contribution to the modulus at low strain increases, it causes larger deviations from the ideal behaviour at higher strain. In the dry state, all the stress data fall on the same curve once normalized by the corresponding moduli that are, of course, very different (Table 1). This unexpected result is likely to be the consequence that for all these networks the entanglement contribution to the modulus according to a NAST analysis (Table 2) is about 50%.

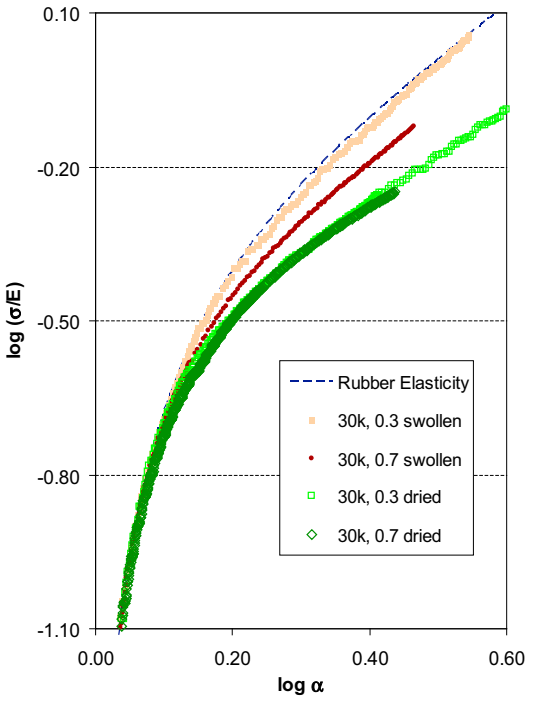

Fig. 2. Results from the 30 k networks.

Table 1
Sample composition and properties.

M_n of precursor chains	Fraction of reactive polymer content in network ϕ	Young modulus of prepared network E_s (MPa)	Young modulus of dried network E_d (MPa)	Soluble fraction W_s (mass%)
10 k	0.3	0.13	0.24	1.5
	0.4	0.23	0.36	0.7
	0.5	0.30	0.45	2.4
	0.7	0.62	0.67	1.3
	0.9	0.84	0.91	0.9
30 k	0.3	0.019	0.064	0.1
	0.4	0.10	0.15	0.7
	0.5	0.11	0.17	1.9
	0.7	0.22	0.26	1.2
	0.9	0.33	0.37	1.0
80 k	0.4	0.038	0.13	2.9
	0.5	0.022	0.17	3.9
	0.7	0.086	0.22	2.5
	0.9	0.25	0.35	2.0

Interpenetration of chains upon drying is much more extensive for the networks prepared in the more swollen state and has led to the larger increase of the entanglement contribution to the modulus even though it does not lead to trapped entanglements. In the swollen networks, these interpenetrated chains disperse and their stress–strain behaviour become closer to the ideal behaviour. The behaviour of the 10 k networks is somewhat analogous to the 30 k networks except that deviations from ideality of the dried networks are much less pronounced than for the 30 k networks.

In Fig. 3 we show the results for networks synthesized with precursor chains of molar mass 80,000 g/mol. The data reported are for networks prepared at the two different reactive polymer concentrations of $\phi = 0.4$ and 0.9. Because the network prepared at $\phi = 0.4$ contains less trapped entanglements, it is seen to follow the ideal rubber elasticity law to higher extension than the network prepared at $\phi = 0.9$. The extent of the deviation from ideality of the dry networks compared to the deviation of the corresponding swollen networks increases (and dramatically more so for the $\phi = 0.4$ network). The difference in the deviation from ideality in the stress–strain behaviour of a network in its swollen state compared to its dry state can be caused by the solvent decreasing the effect of trapped entanglements and of dispersion in the swollen state of no-longer interpenetrated chains. That difference for the $\phi = 0.4$ network between swollen and dry state is expected to be dominated by chain dispersion. For the case of the $\phi = 0.9$ network whose properties are expected to be dominated by trapped entanglements, the difference after solvent extraction is much smaller.

The $\phi = 0.4$ dried 80 k network is expected to have a lower extent of trapped entanglements and greater interpenatration of chains upon drying as compared to the $\phi = 0.9$ sample. Results from the $\phi = 0.5$ and 0.7 samples fall between the data of Fig. 3 and are not shown for clarity. The results from the dried samples of these networks are clearly different from the samples of lower molar mass precursor networks. The stress–strain data of the $\phi = 0.4$ dried sample follow the ideal behaviour to a higher extension ratio than the $\phi = 0.9$ sample and its deviation from ideality at higher extension is smaller. The large molar mass precursor networks have a much higher extent of chain interpenetration upon drying that allows the network to follow the ideal behaviour to higher extension. The difference in behaviour between swollen and dried may be considered to be due primarily to solvent lubrication of trapped entanglements for the 0.9 network but primarily due to chain dispersion for the 0.4 network. Up to an extension of about 60% ($\log \alpha \approx 0.2$), the data from the swollen and dried 0.4 network follow similar behaviour, it is tempting to assume that the large difference

Table 2
Comparison of the Mooney–Rivlin constants with the NAST parameters.

M_n	ϕ	Swollen networks				Dried networks			
		X-link factor		Entanglement factor		X-link factor		Entanglement factor	
		$2C_{1,s}$	$G_{c,s}$	$2C_{2,s}$	$G_{e,s}$	$2C_{1,d}$	$G_{c,d}$	$2C_{2,d}$	$G_{e,d}$
10 k	0.3	0.040	0.041	0.0042	0.0058	0.057	0.052	0.030	0.033
	0.4	0.066	0.063	0.014	0.016	0.085	0.075	0.044	0.056
	0.5	0.092	0.087	0.013	0.018	0.11	0.089	0.051	0.067
	0.7	0.15	0.13	0.069	0.084	0.15	0.12	0.093	0.12
	0.9	0.17	0.15	0.12	0.14	0.19	0.15	0.12	0.15
30 k	0.3	0.0065	0.0055	0.0031	0.0020	0.010	0.010	0.013	0.010
	0.4	0.028	0.027	0.0081	0.010	0.022	0.024	0.035	0.025
	0.5	0.032	0.028	0.0092	0.011	0.029	0.027	0.037	0.033
	0.7	0.049	0.046	0.030	0.029	0.043	0.044	0.051	0.042
	0.9	0.073	0.064	0.041	0.044	0.073	0.066	0.057	0.058
80 k	0.4	0.0076	0.0066	0.0050	0.0054	0.0057	0.0043	0.057	0.044
	0.5	0.0031	0.0024	0.0038	0.0042	0.0042	0.0046	0.058	0.044
	0.7	0.016	0.0087	0.019	0.022	0.017	0.010	0.062	0.066
	0.9	0.030	0.0091	0.059	0.070	0.026	0.010	0.085	0.085

in behaviour beyond log $\alpha = 0.2$ is caused by dispersion of chains that interpenetrated each other during drying.

Quantitative analysis of the data (Section 3.2, Table 2) indicates that the entanglement contribution to the modulus increased almost 10 fold upon drying the $\phi = 0.4$ network, but less than 40% for the $\phi = 0.9$ network. Dispersion of entangled chains that are not hindered by trapped entanglements allows the normalized stress to be reduced more substantially at high strain relative to the normalized stress of the swollen network as compared to the $\phi =$ 0.9 network. The latter is dominated by trapped entanglements and low interspersion upon drying. Note that the 0.4 samples can be extended up to 400% before breaking. It is also important to point out that even at this high extension, the stress of the dry network is well below that of the ideal behaviour indicating that, at the molecular level, the chain are much less stressed than in the swollen situation where the data hint at a stress upturn due to limited chain extensibility [1].

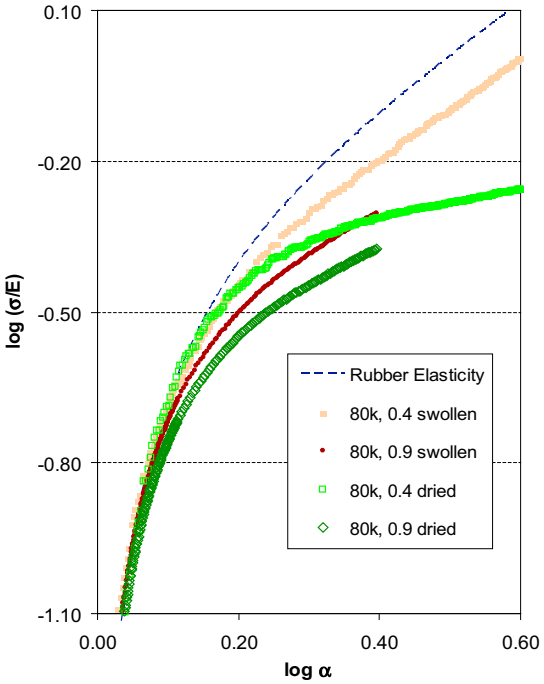

Fig. 3. Results for the 80 k networks.

3.2. Quantitative analysis of stress–strain data

To provide a quantitative basis for the physical interpretation of the stress–strain data presented above, we analyze both extension and compression data from our samples using Rubinstein and Panyukov non-affine slip-tube (NAST) model of elasticity that gives the relation [4,12]

$$F^*\left(\alpha^{-1}\right) = G_c + \frac{G_e}{0.74\alpha + 0.61\alpha^{-1/2} - 0.35} \tag{2}$$

Here $F^*(\alpha^{-1})$ represents the Mooney ratio of the stress σ to the functional dependence $\alpha - \alpha^{-2}$, G_c (contribution of crosslinks to the modulus) and G_e (contribution of "entanglements") are two parameters. The slip-tube model has been shown to provide a good fit to experimental data from uniaxially strained PDMS elastomers [12] and was shown recently to be in very good agreement with molecular dynamics simulations [14]. Using this model allows us therefore to determine how the sample preparation conditions of endlinked elastomers (precursor molar mass and concentration) affect the structure in terms of extent of chemical crosslinks and entanglements. Comparison of stress–strain results from swollen and dried networks further illustrates the role of a solvent in reducing the entanglement contribution to the modulus.

Fig. 4 shows fits of the data from all our samples with different precursor M_n and different initial concentration ϕ. Overall, most of

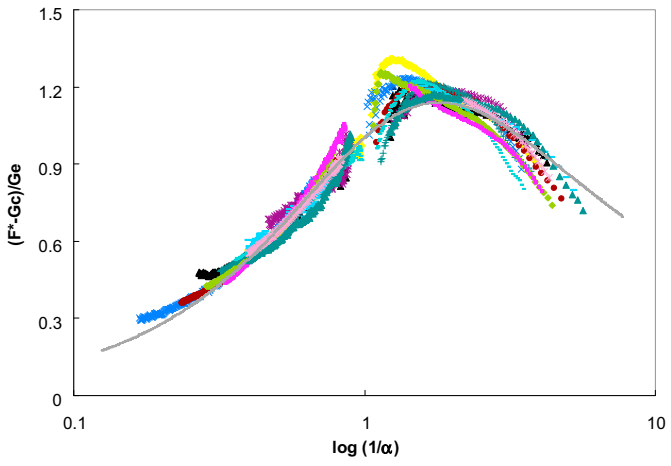

Fig. 4. Fits of all the experimental data to the NAST model represented by the smooth curve.

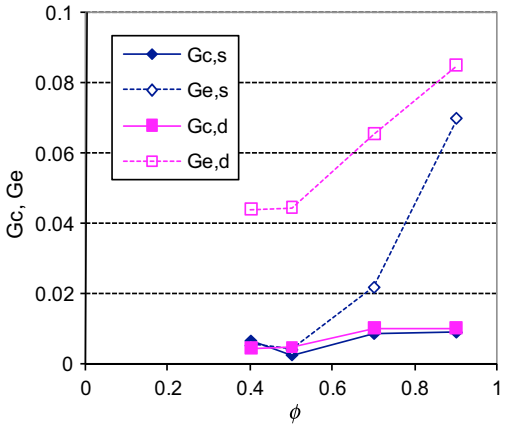

Fig. 5. Values of the NAST model parameters for the 80 k networks (s, swollen and d, dried) as a function of reactive polymer concentration during curing.

our experimental data follow the trends of the model reasonably well with the data from the swollen networks following the model more closely. There are typically large experimental errors around $\alpha = 1$ that explain the deviations there, but there are also some noticeable deviations at high extension and compression. The compression data of the 10 k networks deviate the most. Nonetheless, we used the model to determine its two parameters G_c and G_e from the best fit to the data. These values are listed in Table 2 along with values of the $2C_1$ and $2C_2$ parameters obtained from a fit of the extension data to the well-known Mooney–Rivlin equation (Eq. (3)). The extracted values of G_c and G_e for the networks synthesized with precursor chains of molar mass 80,000 g/mol are plotted in Fig. 5. We observe that: 1) for this high molar mass precursor networks, crosslinking in the presence of the solvent does not change appreciably the contribution to crosslinks in comparison to the large change in the entanglement contribution; and 2) the large difference between $G_{e,s}$ and $G_{e,d}$ come from the interspersion of chains that become "entangled" upon drying. For the $\phi = 0.9$ network, there is a large extent of trapped entanglement contributing to $G_{e,s}$ and little interspersion upon drying. The values of G_c vary little with ϕ for these networks as compared to the 10 k and 30 k networks shown in Fig. 6. The large change in G_c with ϕ in the lower molar mass precursor networks can be interpreted as the formation of inelastic loops (defects) at high solvent concentration during curing in these cases. As a function of the molar mass of precursor chains, one observes an inversion of the relative contributions of G_e and G_c to the total modulus. For the 10 k networks, the crosslink contribution to the modulus G_c is dominant across all ϕ's. The 30 k data show a transition where for the dry networks, values of G_e and G_c are comparable, and finally G_e dominates the modulus of the 80 k networks except at low ϕ for the swollen networks where the two contributions are comparable.

Since the covalent crosslink density does not change as one goes from the swollen state to the dry state, the values of $G_{c,s}$ and $G_{c,d}$ should be identical. As seen in Figs. 5 and 6, the experimentally fitted values are in general quite close. Unlike the values of G_c for the 80 k networks that are relatively small, the corresponding values for the 10 k and 30 k networks are large and vary strongly with ϕ. This is a reflection of the extent of inelastic loop formation for these smaller molar mass precursors [15] that is expected to increase with dilution (smaller ϕ).

Although the initial premise was that the presence of the solvent might affect only the extent of entanglements (G_e) and not the extent of covalently crosslinked elastic chains (G_c), the analysis of the data show that this is not the case except for the 80 k networks prepared at fairly high ϕ ($\geq$0.7).

For comparison, we have also analyzed the uniaxial extension data in terms of the Mooney–Rivlin equation [1,2]:

$$F^*\left(\alpha^{-1}\right) = 2C_1 + 2C_2/\alpha \tag{3}$$

Although this equation is derived from a continuum mechanics approach, the $2C_2$ term has been associated with the "interaction" contribution neglected in the ideal rubber elasticity model because Eq. (3) reduces to Eq. (1) when $C_2 = 0$. The values of $2C_1$ and $2C_2$ for all our samples are listed in Table 2 along with the values of G_c and G_e from fits of both extension and compression data to Eq. (2) of the NAST model.

We note that in general one finds a pretty good agreement between the extracted values of $2C_1$ and G_c on one hand and $2C_2$ and G_e on the other. This obviously lends support to interpreting the C_2 coefficient to a chain "interaction" contribution to the stress–strain behaviour. Since the values of $2C_1$ and $2C_2$ are extracted from a small range of the extension ratio where the linearity of F^* versus $1/\alpha$ is well obeyed, one has a greater confidence in the values extracted in this regime. However, Eq. (3) totally fails to even qualitatively predict the behaviour observed under compression ($1/\alpha > 1$) which is nicely captured by the NAST model [4,12]. On the other hand, because G_c and G_e are extracted by fitting all the experimental data, stress–strain trends at high loadings can lead to rare instances in which the sum of G_c and G_e deviates from the value of the elastic modulus obtained at low strain.

We have also analyzed the data in terms of the Flory–Erman (F–E) model [2] with a two parameter fit representing a crosslink

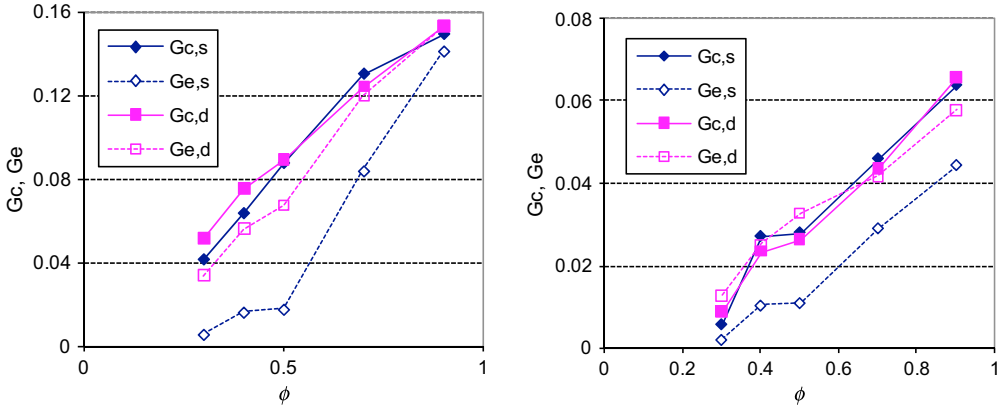

Fig. 6. Values of the NAST model parameters for the 10 k networks (left) and the 30 k networks (right) as a function of the reactive polymer concentration during curing.

contribution to the modulus based on the phantom model and a constraint contribution for the effect of entanglements. Unlike the NAST model, the F–E model does not lead to a master curve where all the data could be fitted to a single master curve. In this case, the shape of the reduced stress $F^*(\alpha^{-1})$ depends on the parameter κ of this model that accounts for the effect of entanglement constraints. The experimental data of only a few samples could be fitted with the F–E model by the selection of appropriate values of the model parameters. Because this model is restricted to a value of the crosslink contribution to the modulus being always greater or equal to the entanglement contribution, it is unable to adequately describe some of the 80 k samples where the entanglement contribution to the modulus is dominant. Extrapolating our results to networks endlinked with infinitely large molar mass precursors, we would expect that their modulus would correspond to the rubbery plateau of the melt due entirely to entanglements with no measurable contribution from crosslinks.

4. Conclusion

We have investigated the role of solvent content, trapped entanglements and chain interpenetration on the deviation at moderate strain levels of the behaviour of uniaxially strained endlinked PDMS networks from the prediction of ideal rubber elasticity. We have synthesized networks with different molar mass precursors in different amount of solvent to show that these deviations do not come only from slippage of trapped entanglement between crosslinks but also from dispersion (un-entangling) of elastic chains that have few or no trapped entanglements between them. We analyzed the experimental data from uniaxially strained samples in terms of the coarse-grained NAST model as well as with the Mooney–Rivlin equation. We find a good correspondence between the coefficients of the continuum model of Mooney and Rivlin ($2C_1$ and $2C_2$) when fitted to the extension data only and the crosslink and entanglement parameters (G_c and G_e) of the coarse-grained molecular model of Rubinstein and Panyukov when fitted over both extension and compression data. The entanglement contribution to the modulus clearly dominates over the entanglement contribution irrespective of the polymer concentration at preparation when the 80 k networks are tested dry. When tested in the prepared swollen state, the crosslink contribution is still dominant for polymer volume fraction equal or greater than 0.7. On the other hand, for the 10 k networks prepared from the lowest molar mass precursors, the crosslink contribution is dominant over the entire spectrum of polymer volume fractions. The 30 k networks present an intermediate situation.

Acknowledgments

We thank Geoff Genesky for several useful discussions and for comments on the manuscript. This work was supported by the National Science Foundation Polymers Program under grant DMR-0705565. We also made use of the Shared Experimental Facilities of the Cornell Center for Materials Research supported through the National Science Foundation Materials Research Science and Engineering Centers Program (Award DMR-0520404).

References

[1] Treloar LRG. The physics of rubber elasticity. 2nd ed. London: Oxford University Press; 1958.
[2] Erman B, Mark JE. Structures and properties of rubberlike networks. New York: Oxford University Press; 1997.
[3] Graessley WW. Polymeric liquids and networks: structure and properties. New York: Garland Science, Taylor and Francis Group; 2004.
[4] Rubinstein M, Panyukov S. Macromolecules 2002;35:6670.
[5] Patel SK, Malone S, Cohen C, Gillmor JR, Colby RH. Macromolecules 1992;25:5241.
[6] Valles E, Macosko C. Macromolecules 1979;12:521.
[7] Meyers K, Bye M, Merrill E. Macromolecules 1980;13:1045.
[8] Sivasailam K, Cohen C. J Rheol 2000;44:897.
[9] Urayama K, Kohjiya S. Polymer 1997;38:955.
[10] Kawamura T, Urayama K, Kohjiya S. J Polym Sci Part B Polym Phys 2002;40:2780.
[11] Lapp A, Herz J, Strazielle C. Makromol Chem 1985;186:1919.
[12] Rubinstein M, Colby RH. Polymer physics. New York: Oxford University Press; 2003.
[13] Takeuchi H, Cohen C. Macromolecules 1999;32:6792.
[14] Svaneborg C, Everaers R, Grest GS, Curro JG. Macromolecules 2008;41:4920.
[15] Gilra N, Cohen C, Panagiotopoulos AZ. J Chem Phys 2000;112:6910.